Mine Water and the Environment (2022) 41:679–694
https://doi.org/10.1007/s10230-022-00885-4

TECHNICAL ARTICLE

Performance of Semi-passive Systems for the Biological Treatment of High-As Acid Mine Drainage: Results from a Year of Monitoring at the Carnoulès Mine (Southern France)

C. Diaz-Vanegas[1,2] · C. Casiot[1] · L. Lin[3] · L. De Windt[4] · M. Héry[1] · A. Desoeuvre[1] · O. Bruneel[1] · F. Battaglia-Brunet[2] · J. Jacob[2]

Received: 2 August 2021 / Accepted: 10 June 2022 / Published online: 4 July 2022

Abstract
Two semi-passive treatment systems for iron (Fe) and arsenic (As) removal in AMD were installed and monitored in-situ for more than a year. These technologies were designed to treat the As-enriched AMD (≈ 1 g/L Fe(II) and 100 mg/L As(III)) of the ancient Carnoulès mine. The treatment was based on biological Fe and As oxidation by indigenous bacteria, and subsequent immobilization of As by ferric hydroxysulfates. Forced aeration and wood/pozzolana or plastic support were used for biofilm attachment. The system performance ranged from 86 to 98% for Fe oxidation, 30 to 60% for Fe removal, and 50 to 80% for As removal at a hydraulic retention time of 9 h. No significant difference were measured between the two biofilm supports. The wood/pozzolana support had a shorter delay for performance recovery after interruptions. Iron oxidation rates were similar to those obtained in the Carnoulès AMD stream and laboratory bioreactor, while As oxidation seemed to be enhanced. The sludge accumulated between 39 and 91 mg/g of As, mainly in the As(V) oxidation state; jarosite and amorphous ferric hydroxysulfate phases were the main Fe and As scavengers. Challenging environmental conditions during the long monitoring period confirm the robustness of the treatment units. The data will be useful in designing future full-scale treatment systems adapted to As-rich AMD.

Keywords Mine waste water · Biological arsenic oxidation · Biological iron oxidation · Bioremediation · Field-pilot

Introduction

Mining activities can adversely affect water resources for decades after mine closure and decommissioning (Neculita et al. 2007; Ribeiro Neiva et al. 2016). The associated oxidation of sulfide minerals and release of acid mine drainage (AMD) into the environment may cause the remobilization of toxic elements such as arsenic (As), contaminating water resources and strongly affecting aquatic ecosystems (Nordstrom and Alpers 1999; Paikaray 2015). In AMD, the two predominant inorganic As species are arsenite As(III) and arsenate As(V); the reduced As(III) form is more mobile than oxidized As(V) due to less retention on solid phases (Tsai et al. 2009). Thus, the predominance of As(III) in some AMD streams further complicates their treatment (Mondal et al. 2006). Despite the threat represented by As-rich AMD to ecosystems and human health, the treatment of these waters remains challenging, especially at high As concentrations (Whitehead et al. 2005).

Nowadays, active chemical treatments such as lime neutralization are the most common strategies implemented in-situ to treat AMD (Wang et al. 2018). The main disadvantages of these chemical neutralizations are their cost, the accumulation of large quantities of polluted sludge, and a labor-intensive maintenance (Habe et al. 2020). In general, chemical neutralization alone has been identified as unsustainable strategy in the long term (Igarashi et al. 2020). Thus, the development of affordable, effective, and

✉ C. Casiot
corinne.casiot-marouani@umontpellier.fr

1 HydroSciences Montpellier, University Montpellier, CNRS, IRD, Montpellier, France

2 Water, Environment, Process and Analyses Division, French Geological Survey (BRGM), Orléans, France

3 LGEI (Laboratoire de Génie de l'Environnement Industriel), Institut Mines-Télécom Alès, Alès, France

4 Centre de Géosciences, MINES ParisTech, PSL University, 77300 Fontainebleau, France

ecological processes to handle these acid effluents is particularly needed, especially for abandoned mines where the use of expensive technologies is not possible. Passive and semi-passive biotechnology based on biogeochemical processes observed in nature can be more sustainable and cost-effective (Sato et al. 2018).

Iron and As bio-oxidation and subsequent mineral precipitation catalyzed by native microorganisms has been reported as a potentially suitable strategy to remove As and Fe from AMD for abandoned mines (Ahoranta et al. 2016; Chen and Jiang 2012; Elbaz-Poulichet et al. 2006; Fernandez-Rojo et al. 2017; Leblanc et al. 2002; Majzlan et al. 2007; Paikaray 2015). The iron bio-oxidation process induces the precipitation of ferric hydroxysulfate minerals that can adsorb or co-precipitate the dissolved As (Majzlan et al. 2016). This process promotes As immobilization by formation of poorly crystalline and/or amorphous phases such as schwertmannite, ferrihydrite, goethite, tooeleite, and amorphous ferric arsenate (Asta et al. 2010a; Carlson et al. 2002). This strategy is based on a natural attenuation process observed and studied in different AMD streams around the world, such as the Iberian pyrite belt in Spain (Asta et al. 2010b) and Reigous Creek (Carnoulès mine) in France (Egal et al. 2010; Morin et al. 2003).

The Carnoulès As-rich AMD gave rise to the Reigous Creek and has been the target of several studies that aimed to develop an in-situ bioreactor to optimize the natural As attenuation process (Bruneel et al. 2003; Casiot et al. 2003; Elbaz-Poulichet et al. 2006; Fernandez-Rojo et al. 2019; Laroche et al. 2018; Tardy et al. 2018). The relevance of this case study is based on the site's challenging conditions, with high and variable As concentration between 50 and 100 mg/L, mainly in the reduced As(III) form, acid pH (3.2–5), and Fe concentration ranging from 500 to 1000 mg/L. The site, which is located in a small valley, and the climate conditions with periodic heavy rainfall, makes it difficult to install and operate treatment facilities (Elbaz-Poulichet et al. 2006).

Experimental and modelling results of batch and flow-through experiments have shown that aeration and biofilm surface area were factors limiting Fe and As removal yields in the treatment of high-As AMD by biological oxidation in our previous laboratory and field pilots (Fernandez-Rojo et al. 2017, 2019; Garcia-Rios et al. 2021). Attempts to increase the surface area of the biofilm using river sand as bacteria growth support in a fully passive field-pilot resulted in rapid clogging. Moreover, the supply of oxygen by simple diffusion at the surface of the thin water film was not sufficient, which dramatically decreased Fe(II) oxidation and provided irregular As removal (Fernandez-Rojo et al. 2019). The use of active aeration and a bacteria growth support with a larger porosity were identified as key elements in the design of future field pilot experiments.

In continuity with these previous laboratory and field pilot experiments, the present study was aimed at: (i) evaluating the on-site performance of a scaled up pilot for biological treatment of high-As AMD (> 50 mg/L of As(III)), under optimized operating conditions (forced aeration, suitable bacterial support, controlled flow rate), and during 1-year monitoring period; the treatment was based on biological Fe oxidation mediated by a native microbial community, and As incorporation into Fe–As solid phases, (ii) comparing two bacterial growth support media, and (iii) evaluating the robustness of the system with respect to temporal variations of AMD physicochemistry, flow, and different environmental conditions.

Methods

Set-up and Operation

Two field-scale systems for the biological oxidation were installed downstream of the Carnoulès tailings dam (southern France) in July 2019. Each system consisted of a 1 m^3 plastic tank filled with different substrate materials (Fig. 1). At the bottom of each tank, a grid with a mesh size of 19 mm was installed to retain the bacteria substrate in the upper part of the tank to reduce the risk of potential clogging of the outlet pipe. Two air diffusers providing aeration at around 300 L/h were installed beneath the grid for each tank. The devices were supplied with the same AMD from Reigous Creek by a continuous flow mechanism controlled by peristaltic pumps.

One device was filled with 6.5 kg of plastic support (Biofill®, Type A) and the other was filled with 174 kg of 80 wt% pozzolana (pozzolanic ash) and 20 wt% wood chips (pine bark sized 20–40 mm, Jardiland®) mixture. The plastic support has been used as a standard in biological water treatments, due to its high porosity (96%), specific surface area (> 160 m^2/m^3), and irregular shape, which allows an optimal biofilm development without clogging problems. The wood/pozzolana mixture has a larger specific surface area (333 m^2/m^3), but a lower porosity (64%). This mixture has been used previously in passive AMD treatments and has demonstrated good hydraulic properties at low-cost (Rötting et al. 2008b).

The two units were supplied with AMD during seven periods (Fig. 2): A, B, C, D, E, F, and G from July 2019 to September 2020. The flow rates were set to 15 or 30 L/h, which corresponds to hydraulic retention times of 17.5 and 8.7 h for the unit with the plastic support (PS) and 19.3 and 9.7 h for the unit with the wood/pozzolana support (WP). The operational phases were determined by changes in flow rate and flow interruptions as well as operational and technical issues. Power supply for the units was changed from a generator to an electrical connection, while pump

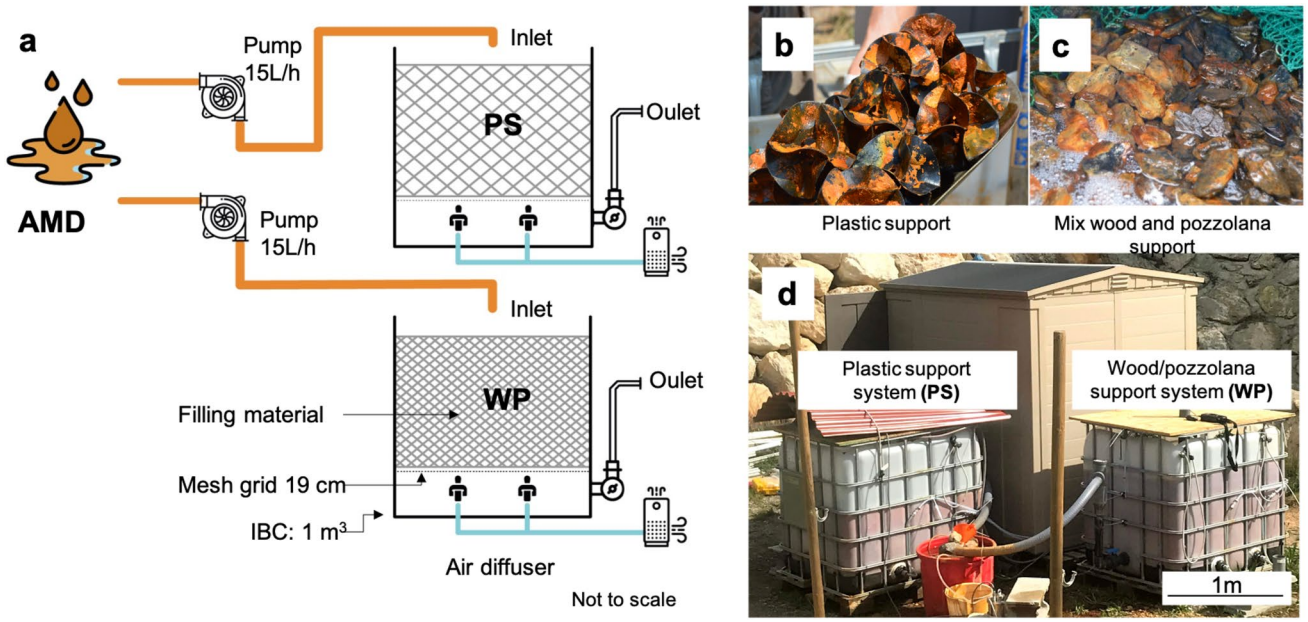

Fig. 1 **a** Schematic representations of the biological oxidative devices, one device filled with a plastic support (PS) and the second device filled with pozzolana and wood mixture (WP), **b** plastic support, **c** wood and pozzolana mixture support and **d** in-situ devices

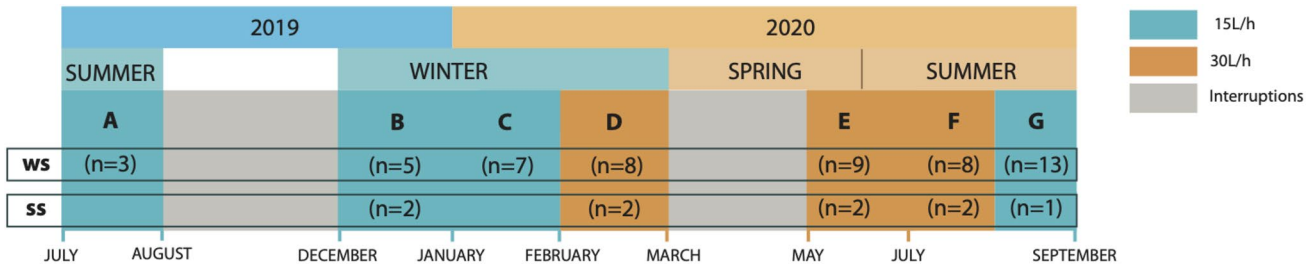

Fig. 2 Timeline of the operation and monitoring of PS and WP treatment devices including, seven periods distributed across seasons, undesired interruptions. The number (n) of water samples (WS) and sludge samples (SS) taken in each period are also indicated

maintenance and a Covid-19 lockdown period interrupted the intervals.

In July 2020 (Period F), clogging of the air diffusers occurred in both units due to the accumulation of a yellowish precipitate in the bottom of the tanks. The air diffusers started working properly again after maintenance in September (Period G).

Water Sampling and Characterization

Water samples were collected two to three times per week at three sampling points: (1) device inlet with the wood/pozzolana support (which was also representative of the inlet water feeding the device with plastic support), (2) device outlet with wood/pozzolana support, (3) device outlet with plastic support. Sludge samples were taken every two weeks on the first ten centimeters inside each unit. The number of sampling campaigns are indicated in Fig. 2: 3 times during period A, 5 times during period B, 7 times during period C, 8 times during period D, 9 times during period E, 8 times during period F and 13 times during period G.

The water samples were preserved and characterized according to the routine procedures described in Fernandez-Rojo et al. (2017). They were split in two sub samples for in-situ and lab measurements. The in-situ physicochemical measurements were conducted using a Hach HQ40D portable multi-meter (i.e. temperature, pH, redox potential, electrical conductivity, and dissolved oxygen concentration). 500 mL of the second subsample was filtered using 0.22 µm cellulose filters. Then, the sample was immediately distributed in different aliquots; one aliquot was diluted in 1% HNO_3 solution (Suprapur quality) for major and trace element analysis, another one was diluted in acetate/acetic acid buffer (pH 4.5) and 0.05% (w:w)

phenanthrolinium chloride solution for ferrous iron (FeII) concentration determination and a third one was added acetic acid (0.087 M) and EDTA (0.5 g/L) for redox As speciation analysis. The samples were temperature stabilized at 4 °C and treated according to the appropriate protocols for specific chemical analysis.

The Fe(II) concentration was quantified by colorimetry using the ortho-phenanthroline method by absorbance at 510 nm with a JENWAY 6320D spectrophotometer (detection limit = 88 µg/L, accuracy = ± 5%). For the major and trace elements determination including total Fe and As concentrations, the samples were analyzed by inductively coupled plasma-mass spectrometry (ICP-MS; Thermo X7 Series) at the AETE-ISO platform, University of Montpellier (France). An external calibration with internal standard correction procedure and international certified reference waters (CNRC SLRS-5, NIST SRM 1643e) were used for quality control.

Samples for arsenic speciation (As(III) and As(V) proportions) were analyzed by anion-exchange chromatography (25 cm, 4.1 mm inner diameter Hamilton PRP-X100 column) using a Spectra Device SCM1000 solvent delivery pump coupled to an ICP-MS.

Sludge and Suspended Particulate Matter Characterization

The precipitate formed during the treatment periods accumulated as sludge onto the filling material, while a small amount was transported with the treated water flow as suspended particulate matter (SPM) in the effluent. Both kinds of solids were analyzed, leading to a total of 9 sludge samples and 11 SPM samples collected at the three monitoring points (influent, PS effluent and WP effluent) at least once for each period of operation.

The SPM fraction was recovered by filtration on cellulose filters (0.22 µm) at the outlet drain of each reactor. After each sampling campaign, the filters were dried under vacuum and stored for further analysis. Sludge subsamples were centrifuged and dried in a glove box under nitrogen atmosphere for subsequent As speciation analysis and mineralogical characterizations. Total Fe and As concentrations in the sludge were determined by ICP-MS after acid digestion, while As speciation in the sludge and SPM was determined by HPLC-ICP-MS after an extraction using orthophosphoric acid (1 M, 85%; Resongles et al. 2016).

Mineral characterization was performed by X-ray powder diffraction (XRD) analyses, using the Co K-α radiation of a Malvern-Panalytical Empyrean diffractometer. Data were collected in continuous mode between 5 and 100°2θ with a 0.026°2θ step, counting around 4 h per sample.

As and Fe Distribution in the Colloidal Fraction

Two water samples in period B and one sample in period E were collected from each of the three sampling points and filtered on-site using 0.22 µm cellulose filters. The filtrates were transported in a cool box to the laboratory within 4 h after collection and then filtered using Vivaspin® 20 Ultrafiltration units. A 100 KDa cutting diameter was used for samples in period B. A 10 KDa cutting diameter was used for samples in period E. The ultrafiltration was done in duplicate; the protocol included centrifugation for 5 min at 5000*g*. Afterwards the filtrated water was analyzed according to the following speciation: Fe(II), total Fe, As(V), As(III), total As.

Relevant Calculations

The hydraulic retention time (HRT) was calculated based on the waterbed volume (L) divided by the input flow rate (L/h). The waterbed volumes of the PS and WP units were 260 and 290 L, respectively. These theoretical hydraulic retention times were used to calculate the Fe(II) oxidation rates as well as Fe and As precipitation rates (in mol L^{-1} s^{-1}). Fe(II) was present only in the dissolved phase while Fe(III) was present both in dissolved and particulate phases. Thus, the rate of Fe(II) oxidation was calculated for each device from the decrease of Fe(II) concentration between influent and effluent, according to the following equation:

$$rFe(II) = \frac{[Fe(II)]_{inlet} - [Fe(II)]_{outlet}}{(HRT)} \quad (1)$$

where $[Fe(II)]_{inlet}$ was the dissolved Fe(II) concentration measured at the inlet of the units. $[Fe(II)]_{outlet}$ was measured at the outlet of the PS or WP units. The rate of Fe and As precipitation was calculated accordingly, by using the total dissolved (< 0.22 µm) Fe and total dissolved As concentrations measured by ICP-MS. The rates were calculated using the concentration values from the stationary phase for periods A, B, C, D, E, and G (except for period F, all data were used). The stationary phase for each period was defined when the performance did not change by more than 10%. For instance, the PS system needed between 5 to 10 days to reach it, while the WP system reached this stationary phase in the first five days.

As(III) and As(V) co-exist both in dissolved and particulate phases. Calculation of the rate of As(III) oxidation was carried out using a mass balance calculation for each unit (see Supplemental Calculation S-1). The mass balance used the concentration of dissolved and particulate As(III) and As(V) species in the inlet and outlet water samples,

together with the amount of As(III) and As(V) retained in the sludge and SPM.

For biological Fe(II) oxidation, a first-order kinetic constant $k_{Fe(II)Field}$ (Larson et al. 2014) was also calculated to compare the unit performances with other studies. The general reaction for biological iron oxidation considered in the present study was:

$$Fe^{2+} + 0.25O_2(aq) + H^+ \rightarrow Fe^{3+} + 0.5H_2O \quad (2)$$

This first order kinetic law assumes that the Fe(II) oxidation rate depends on the dissolved Fe(II) concentration:

$$kFe(II)_{field}(\min^{-1}) = \frac{-Ln\left(\frac{[Fe(II)]_{diss.Outlet}}{[Fe(II)]_{diss.Inlet}}\right)}{HRT \times 60} \quad (3)$$

$[Fe(II)]_{diss.Inlet}]$ corresponds to the dissolved Fe(II) concentration at the inlet of the devices, $[Fe(II)]_{diss.Outlet}]$ is expressed as the dissolved Fe(II) concentration of the PS and WP effluents, and HRT (h) defines the hydraulic retention time calculated for each unit in each period. This simple rate law was preferred to the fourth order kinetic rate law used by Pesic et al. (1989) and Sheng et al. (2017) in controlled laboratory experiments; those authors considered the parameters Fe(II) concentration, oxygen concentration, pH, and bacterial cell concentrations. Here, it was not possible to establish a fourth order kinetic rate law in the field conditions of the present study. The range of variation of inlet water pH was relatively narrow, aeration promoted fully oxygenated conditions, and it was not possible to quantify Fe-oxidizing bacterial cell counts among the whole autochthonous bacterial community.

Statistical Analysis

Data were analyzed by the non-parametric Mann–Whitney test for significant performance differences in the two support substrates. The Pearson test was used to evaluate the correlation between independent variables; the p-values were obtained at the level of $p < 0.05$. The statistical analyses and graphs were performed with the free R software (http://www.r-project.org/), version 1.2, using the tidyverse and vegan packages and XLSTAT.

Geochemical Model and Thermodynamic Data

The saturation indices (SI) of As and Fe solid phases with respect to the inlet/outlet water chemistry were calculated with the geochemical module CHESS of the HYTEC code (van der Lee et al. 2003) using the truncated-Davies activity correction model and the thermodynamic database (Blanc et al. 2012) version of 2017. The Fe(III)/Fe(II) and As(V)/As(III) oxidation state couples were decoupled from the calculations. Two additional data sets were considered for the sake of consistency with a previous modeling study of lab experiments on Carnoulès AMD microbial treatment (Garcia-Rios et al. 2021). The thermodynamic constants of an amorphous Fe(III)-arsenate (AFA) was adjusted on the batch and flow-through data. The thermodynamic constant of a more soluble and hydrated form of schwertmannite (Sánchez-España et al. 2011) was found to better fit the same experimental data than the original Thermoddem equilibrium constant.

SI values are good indicators for estimating the saturation state of complex aqueous solution such as the present AMD waters vs. mineral reactivity. SI values between −0.5 and 0.5 mean that the solid phase is close to thermodynamic equilibrium. A positive SI value indicates that the solution is oversaturated and that the solid phase can precipitate from the solution. A negative SI means that the solid phase cannot precipitate but can possibly dissolve if in contact with water.

Results

Aqueous Chemistry

Variations of the main physicochemical parameters of the water at the inlet and outlets of the treatment units are presented in Fig. 3 and supplemental Table S-1. The inlet revealed a pH range from 3.2 to 5.1 along one year of operation (Fig. 3a). Those values systematically decreased to 2.8 ± 0.3 on average through the PS and WP units (Fig. 3a). The temperature of the inlet water showed some variability across seasons. Recorded temperatures during summer obtained an average value of 24 ± 4 °C and a maximum of 27 °C in periods A, F and G, whereas recorded temperatures during winter times were obtained with an average around 12 ± 3 °C, and a minimum temperature of 5 °C in periods B and C (Fig. 3b). The variation between the inlet and outlets was no more than 6 °C (Fig. 3b, supplemental Table S-1). The conductivity at the inlet ranged from 2300 to 4270 µS/cm, with the highest values during summer (periods A, F and G) and the lowest during winter (B and C). It decreased by no more than 20% between inlet and outlets (Fig. S-1). The average dissolved oxygen (DO) concentration at the inlet ranged between 6 ± 2 mg/L and showed high variability (high SD values) within each period (Fig. 3c). It increased between inlet and outlets in periods B, C, and D while it did not significantly change in periods A, E, F, and G. Discrete DO measurements were made in the middle of the reactor bed. These DO values were similar to those in outlet water in periods B and C but were lower in periods D and F in both WP and PS units. This lower DO levels marked a time period when consumption exceeded oxygen supply in the reactor bed.

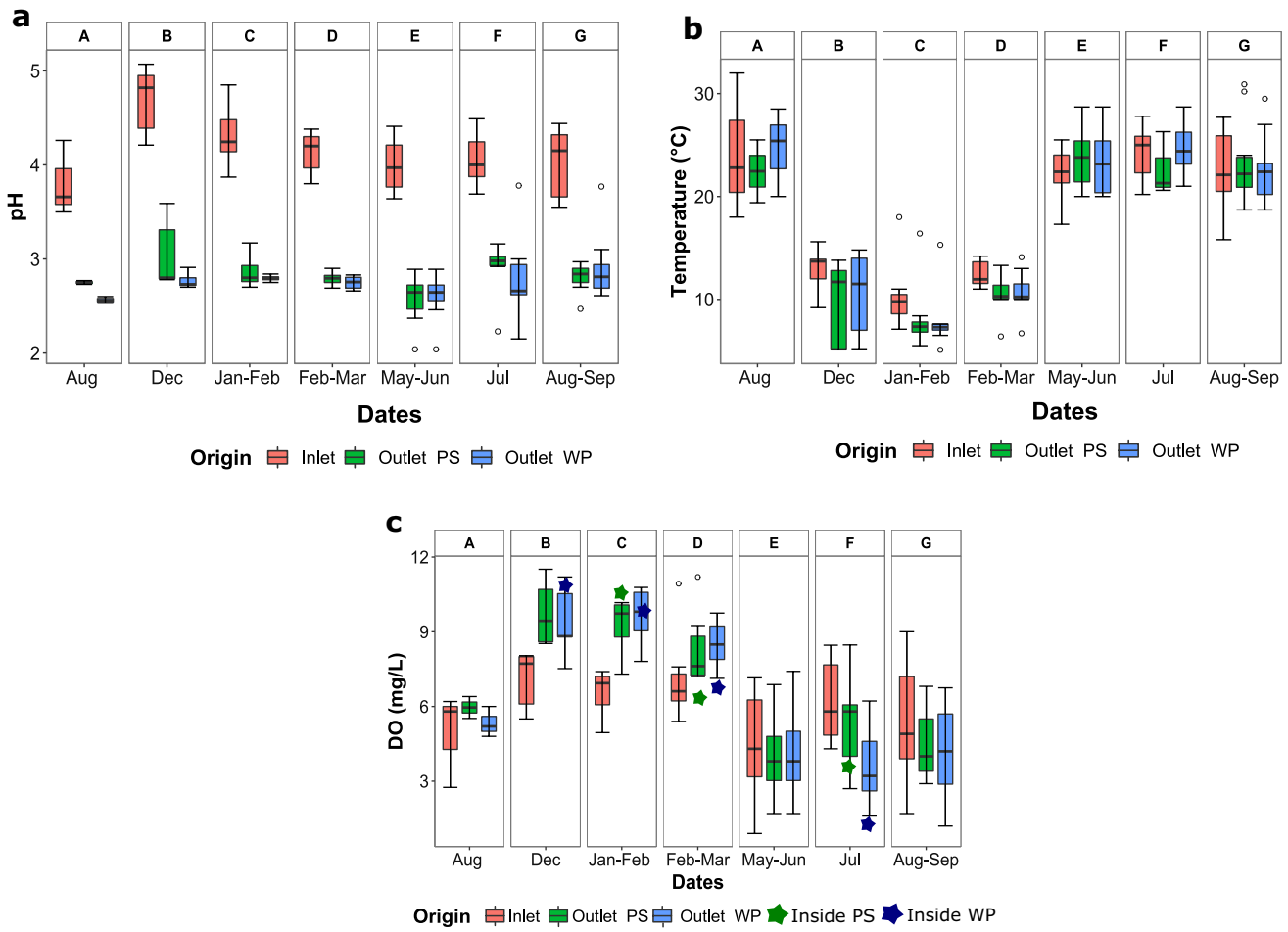

Fig. 3 Boxplot representation of the main physicochemical parameters measured in the inlet water and in the outlet water from the PS and WP devices during seven periods of monitoring, **a** pH, **b** temperature and **c** dissolved oxygen concentration (DO). The dot (°) represents the outliers. The inlet flow used for the different periods were 15L/h for A, B, C and G while 30L/h for D, E and F

Dissolved Iron Concentrations (Total Fe and Redox Species)

Total dissolved Fe concentration, i.e. the sum of dissolved Fe(II) and dissolved Fe(III) in the inlet water, ranged from 300 to 1000 mg/L. The highest concentrations correlate with droughts during summer time (A, E, F and G periods, Fig. 4a). The total dissolved Fe concentration decreased by 20 to 70% between inlet and outlets for most periods (A–E), except period F and early period G.

Ferrous iron concentrations dominated compared to Fe(III) in the inlet water, representing about 90% of the total dissolved Fe (Fig. 4a, b). As indicated in Fig. 4b, the Fe(II) concentration at the inlet decreased from period A (Jul. 19) to period B (Dec. 19) and then gradually increased until period F (Jul. 20). The Fe(II) concentration then decreased between inlet and outlets (Fig. 4b) while the Fe(III) concentration increased (Fig. 4c), indicating the oxidation of Fe(II) in both units. For the PS unit, the Fe oxidation efficiency varied from 60 to 98% in periods A–E, while it always exceeded 90% in these periods in the WP unit. Interruptions of operability occurred in both units between periods A and B and between periods B and C, which led to a temporary decrease of Fe oxidation rate down to 50% in PS unit during the first ten days after restart (Fig. 4b, c) while the WP unit recovered its efficiency shortly (in 3 to 5 days). In period F, outlet Fe(II) concentrations increased substantially in both units, and outlet Fe(III) concentration decreased (Fig. 4b), confirming a decreased Fe oxidation efficiency during the time period when the air diffusers were clogged. After maintenance of the aeration system in late period G, outlet Fe(II) concentrations steeply declined, reflecting a recovery of unit performances.

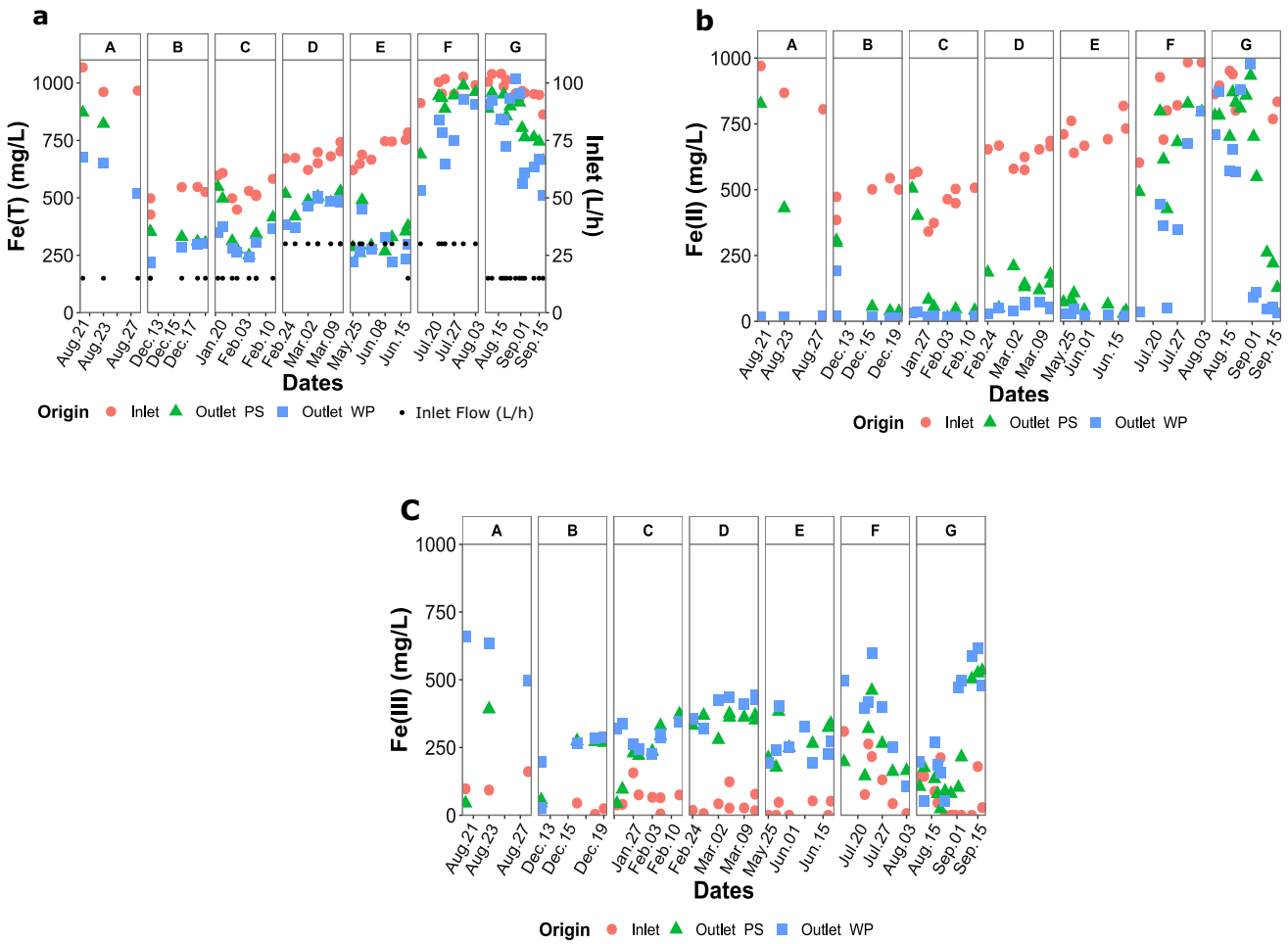

Fig. 4 Variations of the dissolved iron concentration at the inlet and outlet sampling points, for the device with plastic support (PS) and wood/pozzolana support (WP). **a** Total dissolved iron (Fe Total), **b** Ferrous iron (Fe(II)) and **c** ferric iron (Fe(III)). Data collected during seven periods of monitoring: A (Jul.–Aug. 19), B (Dec. 19), C (Jan.–Feb. 20), D (Feb.–Mar. 20), E (May–Jun. 20), F (Jul.–Aug. 20) and G (Aug.–Sep. 20). The inlet flow used for the different periods were 15L/h for A, B, C and G while 30L/h for D, E and F represented with black dots in **a**

Dissolved Arsenic Concentrations (Total As and Redox Species)

Total dissolved As concentration at the inlet varied across the seasons concomitantly to total dissolved Fe concentration (Fig. 5a). It increased from 40 to 70 mg/L during the colder and rainy periods (B, C and D) to 80–100 mg/L during hot periods accompanied by draughts (A, E, F and G). As(III) represented 75 ± 5% of total dissolved As at the inlet (Fig. 5b).

Total dissolved As concentration decreased to a minimum of 10 mg/L at the outlets sampling points for both PS and WP units during periods B, C, E, G, which corresponded to a 50–80% As removal (Fig. 5a). Both As(III) and As(V) concentrations exhibited a decrease between inlet and outlets (Fig. 5b, c). Outlet As(V) concentration punctually exceeded its inlet value in periods A, E and G (Fig. 5c).

Rates of Fe and As Oxidation and Precipitation

The rates of Fe and As oxidation and precipitation in each period (Table 1, supplemental Figs. S-2, S-3, and S-4) were calculated under stationary phases (≈ 10 days after restart) for each unit. The rate of Fe (II) oxidation ranged from 0.8×10^{-7} to 3.3×10^{-7} mol L^{-1} s^{-1} (Table 1, supplemental Fig. S-2); it was nearly two times lower for Fe (III) precipitation, from 0.4×10^{-7} to 2.1×10^{-7} mol L^{-1} s^{-1} (Table 1, supplemental Fig. S-3) and one order of magnitude lower for As precipitation, from 0.7×10^{-8} to 2.6×10^{-8} mol L^{-1} s^{-1} (Table 1, supplemental Fig. S-4). The highest rate values for Fe oxidation and precipitation were observed in period E, compared to the highest rate values of As precipitation that were reached in periods E and F (Table 1, supplemental Fig. S-2 and Fig. S-4). In periods B to E, As removal rate correlated well to the rate of Fe precipitation ($r^2 = 0.98$; Fig.

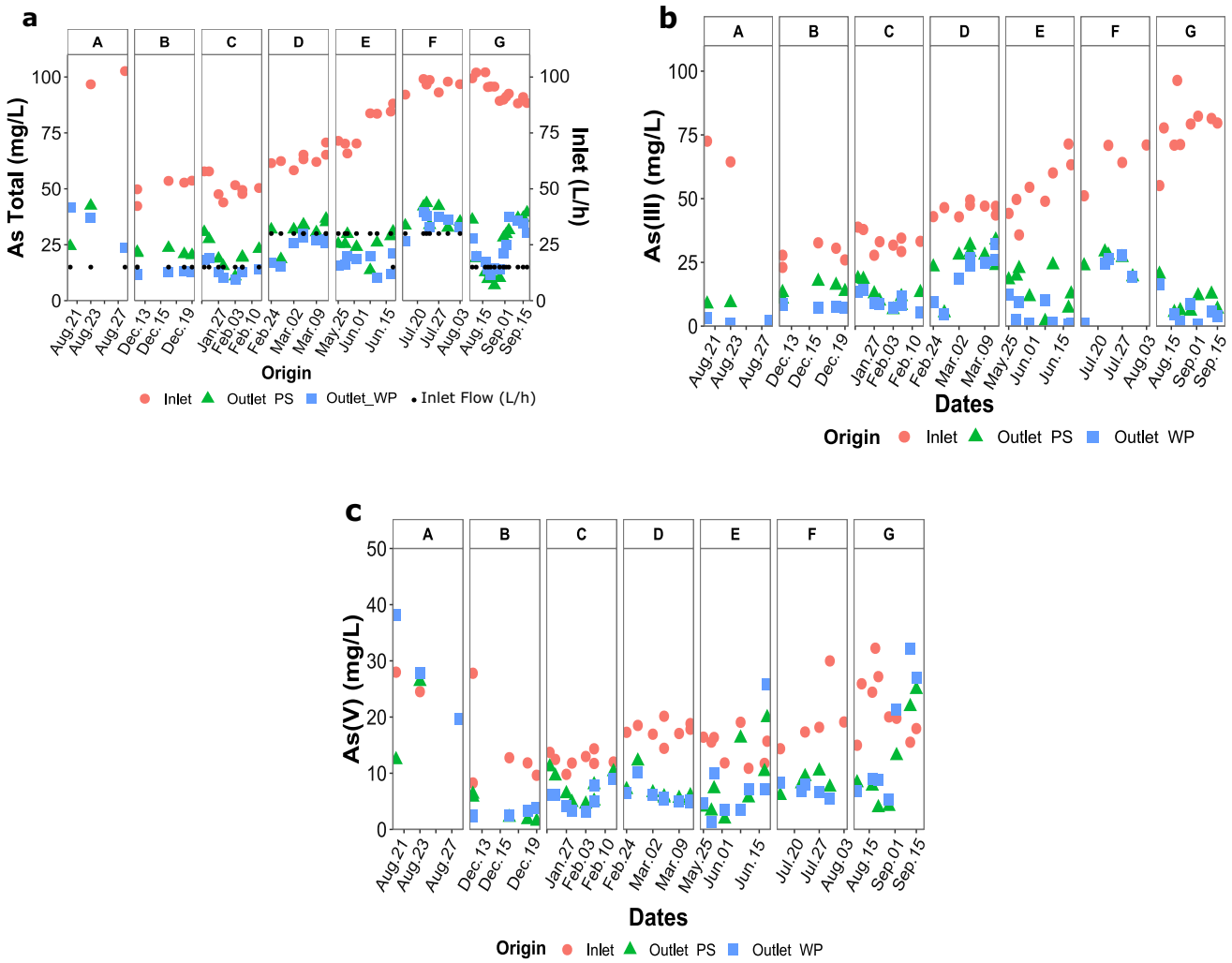

Fig. 5 Variation of the concentration of **a** total dissolved (As Total), **b** arsenite (As(III)) and **c** arsenate (As(V)) at the inlet and outlet sampling points for the device with plastic support (PS) and wood/pozzolana support (WP) during the different periods of operation. The inlet flow used for the different periods were 15 L/h for A, B, C and G while 30 L/h for D, E and F represented with black dots in **a**

Table 1 Rates of Fe oxidation, Fe precipitation, As oxidation and As precipitation ($\times 10^{-7}$ mol L^{-1} s^{-1}) for the PS and WP treatment devices under stationary phases in each period. Average (standard deviation, STD)

	Fe oxidation		Fe precipitation		As oxidation		As precipitation	
	PS	WP	PS	WP	PS	WP	PS	WP
A	0.8 (0.6)	2.2 (0.2)	0.5 (0.1)	1.0 (0.2)	NA	NA	0.15 (0.05)	0.13 (0.02)
B	1.3 (0.1)	1.3 (0.1)	0.64 (0.03)	0.63 (0.05)	< 0.05	< 0.05	0.070 (0.004)	0.080 (0.001)
C	1.3 (0.1)	1.1 (0.2)	0.6 (0.2)	0.56 (0.09)	NA	NA	0.07 (0.01)	0.07 (0.01)
D	2.8 (0.2)	3.0 (0.2)	1.0 (0.2)	1.1 (0.3)	< 0.05	< 0.05	0.13 (0.01)	0.15 (0.02)
E	3.3 (0.1)	3.3 (0.7)	2.1 (0.7)	2.1 (0.6)	< 0.05	0.1	0.22 (0.01)	0.22 (0.05)
F	0.9 (0.5)	2 (1)	0.4 (0.4)	0.9 (0.5)	0.08 (0.02)	0.1 (0.06)	0.26 (0.04)	0.24 (0.05)
G	1.8 (0.4)	2.2 (0.3)	0.56 (0.02)	0.83 (0.09)	0.1	0.1	0.11 (0.01)	0.100 (0.004)

NA not available data, $< 0.05 \times 10^{-9}$ defined as quantification limit for the As oxidation estimation. The inlet flow used for the different periods were 15L/h for A, B, C and G while 30L/h for D, E and F

S-5) and also to inlet water As concentration ($r^2 = 0.89$; supplemental Fig. S-6). The As/Fe molar ratio in the precipitate, calculated from As and Fe removal, averaged 0.13. Such dependency implies a control by As sorption or incorporation into Fe minerals. A similar kinetic dependency was reported by Asta et al. (2010a, b) in AMD from the Iberian

Pyrite Belt. In periods F and G, the As removal rate was not correlated to the rate of Fe precipitation; the As/Fe molar ratio exceeded 0.2 due to slower Fe removal (Fig. S-7).

Mass balance calculations using dissolved and particulate As speciation data (Fig. 5b, c; Table 2) provided an estimation of As oxidation rate in each unit (Table 1). This calculation was based on the assumption that SPM in outlet water reflected the composition of the precipitate that forms at the time of outlet water sampling. The estimation of As oxidation reached its maximum rate (10^{-8} mol L^{-1} s^{-1}) during periods F and G for both units, while during periods B and D, the As oxidation rates were both below the detection limit ($< 0.5 \times 10^{-8}$ mol L^{-1} s^{-1}). Thus, depleted aeration conditions in periods F and G were not a limiting factor for As oxidation in the units.

Under steady state conditions and optimal performances of the aeration system (periods A–E), the average rates of Fe oxidation and precipitation, and As precipitation were statistically similar for the WP and PS units (p-value > 0.05, Mann–Whitney); however, if the surface area is considered for each support substrate (28 m^2 for the PS unit, 54 m^2 for the WP unit), the maximum precipitation rates in grams of Fe and As precipitated per m^2 of support substrate and per day were twice as high for the PS unit (20.2 g m^{-2} d^{-1} for Fe oxidation, 12.4 g m^{-2} d^{-1} for Fe precipitation and 2.1 g m^{-2} d^{-1} for As precipitation) than for the WP unit (10.8 g m^{-2} d^{-1} for Fe oxidation, 6.99 g m^{-2} d^{-1} for Fe precipitation and 1.09 g m^{-2} d^{-1} for As precipitation).

Suspended Particulate Matter in Outlet Water

The amount and composition of the particulate phase in outflow effluents were determined (Table 2). The concentration of SPM ranged from 2 to 124 mg/L. Particulate Fe represented a maximum of 4 wt.% of total (dissolved + particulate) Fe concentration and particulate As represented a maximum of 8% of total (dissolved + particulate) As concentration (Table 2). Thus, this amount of particulate As flowing out of the unit is substantial. In the fraction below 0.22 µm, the colloidal Fe and As fractions (> 100 kDa, measured in period B) represented a maximum of 2% of total (dissolved + particulate) Fe concentration and 9% of total As concentration (Table S-2). Ultrafiltration at 10 kDa (measured in period E) indicated the presence of fine colloids that accounted for up to 32% of total (dissolved + particulate) Fe and 68% of total As. The occasional presence of colloidal Fe and As in the outflow fluid may reflect a rapid formation process. Colloid formation might have occurred directly in the fluid phase rather than at the surface of the biofilm due to specific gradients and oversaturation.

The As/Fe molar ratio in SPM (> 0.22 µm) varied from 0.02 to 0.3 in periods B to E; it increased up to 0.9 in the WP

Table 2 Concentration of SPM (SPM > 0.22 µm), concentration of particulate Fe and As in outlet water (expressed in mg/L and in proportion of total (dissolved + particulate) Fe and As (wt%), and composition of SPM (As/Fe molar ratio, proportion of particulate As(III) and As(V) to total particulate As (wt%))

	Dates (d/m/y)	Device	SPM (mg/L)	Fe (mg/L) (wt% Tot. Fe)	As (mg/L) (wt% Tot. As)	As/Fe (mol/mol)	As(III)/As wt%	As(V)/As wt%
B	12-12-2019	PS	NA	NA	NA	NA	NA	NA
		WP	NA	NA	NA	NA	NA	NA
	19-12-2019	PS	6	2 (0.5%)	0.3 (2%)	0.1	70	30
		WP	2	0.1 (0.04%)	0.01 (0.1%)	0.1	–	100
C	06-02-2020	PS	15	2 (1%)	0.4 (2%)	0.1	41	59
		WP	3	0.2 (0.1%)	0.04 (0.3%)	0.1	26	74
D	05-03-2020	PS	28	8 (1%)	1 (3%)	0.1	76	24
		WP	59	13 (3%)	2 (8%	0.1	69	31
	12-03-2020	PS	43	14 (3%)	1 (1%)	0.03	77	23
		WP	7	3 (0.6%)	0.1 (0.3%)	0.02	47	53
E	29-05-2020	PS	49	11 (2%)	2 (5%)	0.1	58	42
		WP	2	0.2 (0.03%)	0.02 (0.1%)	0.1	3	97
	18-06-2020	PS	28	3 (0.7%)	1 (4%)	0.3	26	74
		WP	9	3 (0.8%)	0.4 (2%)	0.1	9	91
F	23-07-2020	PS	124	35 (4%)	2 (5%)	0.04	58	42
		WP	14	4 (0.5%)	1 (3%)	0.2	22	78
	27-07-2020	PS	NA	NA	NA	NA	NA	NA
		WP	NA	NA	NA	NA	NA	NA
G	15-09-2020	PS	5	0.7 (0.1%)	0.1 (0.3%)	0.1	8	92
		WP	57	0.2 (0.03%)	0.2 (1%)	0.9	12	88

The inlet flow used for the different periods were 15L/h for B, C and G while 30L/h for D, E and F

NA not available data

unit in period G. As(V) represented 23 to 92% of particulate As concentration; the ratio was generally higher in the SPM from the WP system than those from the PS system, except in period G, where both exhibited high As(V) percentage (≥ 88%).

Sludge Composition

Table 3 lists the measured concentrations of total Fe, total As, As(III), As(V), and total Sulphur (S) in the sludge at different periods of operation. The sludge contained 19 to 31 wt% Fe, 4 to 11 wt% As and 3.5 to 5.4 wt% S (dry wt.). In each period, the WP sludge contained slightly lower As and Fe contents (5 ± 1 wt% As and 21 ± 7 wt% Fe) compared to the PS sludge (8 ± 1 wt% As and 27 ± 4 wt% Fe). The As/Fe molar ratio varied from 0.24 to 0.5 in both units, with the highest ratio obtained in period G. Arsenate systematically predominated in the sludge; it represented in average 84 ± 5 wt% of the total As concentration among periods B, E, F and G; it did not exceed 64 ± 7 wt% of the total As concentration during period D. XRD analysis revealed the presence of jarosite, gypsum and quartz, but did not present other well crystallized Fe(III)-As phases (Table 3, supplemental Fig. S-8). The morphology of the sludge differed between the two systems: the sludge from the PS system was more compact and attached to the bacteria growth support, it was more homogenously distributed inside the unit. Conversely, the sludge from the WP system contained more fluid (watery) and was easily transported to the bottom of the pilot where it settled.

Calculated Saturation Indices of Fe–As Phases

Table 4 plots the saturation indices (SI) of the main representative ferric hydroxysulphate and Fe–As phases in the inlet and outlet PS and WP effluents during four periods (B, C, E, and F). They generally exhibited values indicating oversaturation with regards to schwertmannite, jarosite, and scorodite in both inlet and outlet effluents. The substantial decrease in pH during the treatment lowered the SI of all Fe(III)-containing phases due to their high solubility dependency with pH. The pH decrease was caused by the precipitation of potassic jarosite (K-jarosite) and/or schwertmannite due to the oxidation of Fe(II) to Fe(III) by bacteria. The SI values were, however, still positive, which demonstrates that their precipitation was under kinetic control (i.e. thermodynamic equilibrium had not been achieved yet) with respect to the characteristic HRT. Figure 6 plots the evolution of the SI of K-jarosite and schwertmannite vs. pH of the outlet effluents. The observed trend clearly indicates that jarosite and schwertmannite could co-precipitate, and that the precipitation of jarosite will be promoted at pH around 2.7–2.8.

Table 3 Average concentration (% dry wt.) of total Fe, total As, As(III), As(V), total S, their ratios, and the minerals identified by XRD in the sludge sampled in each period

Period	device	n	Total As (wt. %)	Total Fe (wt%)	Total S (wt. %)	As/Fe molar ratio	Fe/S molar ratio	As(III) (wt%)	As(V) (wt%)	pH	Crystallyzed phases
B	PS	2	9 ± 3	31 ± 6	5.2	0.4 ± 0.2	12.4	17 ± 4	83 ± 4	2.8	Jarosite
	WP	2	4 ± 0.3	19 ± 4	3.5	0.3 ± 0.3	10.9	9 ± 4	91 ± 4	2.7	Jarosite
D	PS	2	7 ± 2	31 ± 5	5.3	0.28 ± 0.1	11.8	36 ± 7	64 ± 7	2.7	Jarosite/Quartz
	WP	2	4 ± 1	24 ± 6	4.7	0.24 ± 0.03	10.4	40 ± 10	60 ± 10	2.7	Jarosite/Quartz
E	PS	2	8 ± 1	31 ± 5	5.3	0.34 ± 0.03	12	23	77	2.5	Jarosite/Gypsum/*
	WP	2	6 ± 2	29 ± 3	5.4	0.29 ± 0.1	10.3	20 ± 2	80 ± 2	2.6	Jarosite
F	PS	2	7 ± 1	27 ± 3	4.3	0.36 ± 0.02	12	18 ± 1	82 ± 1	2.9	NA
	WP	2	6 ± 1	29 ± 2	5.0	0.26 ± 0.1	9.9	18 ± 1	82 ± 1	2.7	NA
G	PS	1	11	27	4.6	0.5	12.7	8	92	2.7	Jarosite
	WP	1	7	19	4.6	0.5	9.5	6	94	2.6	Jarosite

NA not available data

*Quartz, the inlet flow used for the different periods were 15L/h for B, C and G while 30L/h for D, E and F

Table 4 Saturation indices calculated from water samples at inlet and outlets with wood/pozzolana support (WP) and plastic support (PS); Thermoddem database, with some additional data (see "Methods")

	19 Dec (period B) Inlet/PS/WP	12 March (period C) Inlet/PS/WP	18 June (period E) Inlet/PS/WP	23 July (period F) Inlet/PS/WP
K-Jarosite(cr)	9.8/6.2/5.7	10.1/6.4/6.3	8.9/4.8/4.5	12.5/7.2/6.1
Schwertmannite[a]	27.3/6.4/4.2	21.8/ 5.8/5.7	17.2/−0.6/0.8	29.7/7.1/3.7
Scorodite(cr)	4.6/1.9/2.3	4.1/2.5/2.4	4.1/0.1/3.1	4.8/3.1/2.8
Scorodite(am)	1.9/−0.7/−0.4	1.5/−0.2/−0.3	1.3/0.1/0.3	2.0/0.3/−0.04
AFA[b]	2.7/0.0/0.3	2.2/0.6/0.5	2.1/0.9/1.1	2.8/1.0/0.7

[a]Sánchez-España et al. (2011)

[b]Amorphous Ferric Arsenate, Garcia-Rios et al. (2021)

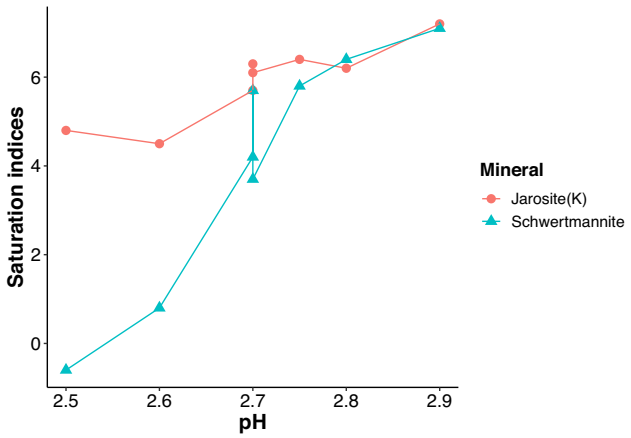

Fig. 6 Evolution of saturation indices of jarosite (round symbols) and schwertmannite (triangle symbols) from outlet water samples, calculated with CHESS

The concentration of K^+ is derived from the Carnoules' AMD (inlet concentration: 19 ± 3 mg/L), 39 ± 29% of the potassium entering the units was removed in the treated water and contributed to the K-jarosite formation. However, this phase was not dominant in our units, since the Fe/K molar ratio in the precipitate was 51 ± 33, whereas Fe(mol)/K(mol) = 3 in K-jarosite.

As(V) solubility in the outlet waters was likely controlled by an amorphous ferric arsenate (AFA), as indicated in Table 4. The SI values of amorphous scorodite (from Thermoddem) and AFA (from Garcia-Rios et al. 2021) were within the range −0.5 to 0.5 (i.e. at equilibrium).

Discussion

General System Performance Compared with Previous Systems

The physico-chemistry of the AMD during the monitoring (pH of 3.2–5, As(III) concentrations of 42–102 mg/L and Fe(II) concentrations of 430–1000 mg/L) was similar to long-term observation data at the Carnoulès site (OREME Observatory, https://oreme.org/). Under steady-state conditions, the treatment units oxidized on average 92 ± 6% of the Fe(II) and removed 43 ± 11% Fe and 67 ± 10% As at a HRT of 9 h. These performances were higher and more stable than those obtained with our previous field bioreactor (Fernandez-Rojo et al. 2019). This previous system functioned entirely under passive conditions, i.e. aeration was provided by simple oxygen diffusion through a thin water film. As a result, Fe oxidation and removal did not exceed 20% while As removal varied widely between 3 and 97%. For comparison, this previous system reached 40% As removal at a similar HRT (10 ± 1 h). The present systems showed similar performance than those obtained in our lab-scale bioreactor that did not use bacterial growth support neither active aeration but a thin water film (4 mm) flowing at the surface of the Fe(II)-oxidizing biofilm. In that passive lab-scale bioreactor, we obtained a maximum of 80% Fe(II) oxidation, 50% Fe removal, and 65% As removal at a HRT ≈ 8 h (Fernandez-Rojo et al. 2017). Thus, the thin water film configuration in the lab-scale bioreactor was efficiently compensated by the use of a bacterial growth support (promoting mass transfers between the solution and the biofilm) and active aeration (promoting oxygen supply to the biofilm) in the present units. Considering the capacity of the lab-scale pilot (0.24 L) and field units (263 or 290 L), a scale-up by a factor of more than a thousand was successfully achieved in the present study, while maintaining the performances of the treatment process.

The rates of Fe oxidation in the present units (1×10^{-7} to 4×10^{-7} mol L^{-1} s^{-1}) were in the low range of literature values (1.5×10^{-7} to 40×10^{-7} mol L^{-1} s^{-1}) for laboratory Fe oxidation bioreactors treating As- and Fe-rich AMD at pH 3.2–5 (Ahoranta et al. 2016; Sheng et al. 2017). The kinetic constant k-value was determined considering a first order kinetics approach toward Fe(II) concentration (Eq. 2) We obtained a kinetic constant k-value of k = 0.003 ± 0.0009 min^{-1} under steady-state conditions in operation periods A–E (Fig. S-9), which corresponds to half-life of 3.7 h. This k-value fitted with those obtained in AMD streams at pH 3.5–4.2 reported for several AMD in the US

and Spain (Larson et al. 2014). This suggests that biological Fe(II) oxidation by the autochthonous microbial community of the Carnoulès AMD was well reproduced in the present treatment units but not enhanced compared to AMD stream conditions. Regarding As removal rates, the present study observed 0.5×10^{-8} to 3×10^{-8} mol L^{-1} s^{-1}, which was similar to our previous field-pilot rates (1×10^{-8} to 2×10^{-8} mol L^{-1} s^{-1}; Fernandez-Rojo et al. 2019) and lab-scale experiments rates (2×10^{-8} to 5×10^{-8} mol L^{-1} s^{-1}; Fernandez-Rojo et al. 2017). The reproducibility of these rates from one pilot to another suggests their ability for future upscaling to full-scale treatment facilities. Regarding As oxidation, 60 to 95% of the As was present as As(V) in the sludge, showing a higher As(III) oxidation yield in the field pilot than in our previous lab-scale experiment in which As(V) reached 48–84% (Fernandez-Rojo et al. 2017, 2018). High oxidation yields were also observed in our previous field pilot where As(V) ranged from 19 to 99% (Fernandez-Rojo et al. 2019). The reason for such differences in As oxidation efficiency between laboratory and field conditions deserves further research.

Effect of the Biofilm Support

The two materials used as biofilm support did not show major differences in term of outlet water hydrochemistry, sludge mineralogy and overall performances. The main difference was the duration of the lag phase regarding Fe(II) oxidation in the early days after restart. The WP system had a shorter lag period than the PS system. This might be associated with the porosity of the wood material providing micro-niches favorable for maintaining an active microbial community (Rötting et al. 2008a). The WP unit showed higher robustness at shutdowns than the PS unit. The lower SPM concentration found in the WP effluent than in the PS effluent might be due to a better SPM settling in the unit containing a mixture of mineral and wood. The relatively high SPM concentration in the PS effluent (up to 0.13 g/L) would require the use of a settling pond downstream of the treatment unit. The WP sludge contained slightly lower As and Fe concentrations compared to the PS sludge, which suggests a dilution by wood debris from the bacteria growth support in the WP unit. The disaggregation of the wood support may be an important issue in the perspective of long-term treatment and sludge disposal.

The As(V) to total As ratio in the SPM was higher in the WP unit than in the PS unit. This may suggest faster As(III) oxidation in the WP unit. The difference did not persist in the sludge due to an aging effect. The wood material provided organic matter that could favor As-oxidizing bacterial populations. An input of nutrients stimulated As(III)-oxidizing bacteria in a batch experiment performed with Carnoulès AMD (Tardy et al. 2018). Occasional measurements of total organic carbon in the PS and WP systems indicated higher concentrations in the WP sludge (71 ± 47 g/kg) than in the PS sludge (3 ± 0.7 g/kg (dry wt.)), although the difference was minor in the treated water (effluent water WP: 5 ± 2 mg/L; PS: 3 ± 1 mg/L). Further research on As-oxidizing gene expression will be necessary to find a possible role of bacterial growth support on As oxidation rate in the units.

Robustness of the System Towards Variations of Operating Conditions

An important factor regarding pilot performance was related to air injection. Dissolved oxygen concentration plays both a direct and indirect role on biological Fe(II) oxidation. First, it is one of the factors that directly controls the rate of Fe(II) oxidation. Second, the DO concentration strongly influences the structure of the Fe-oxidizing bacterial community (FeOB), which consists of species exhibiting different specific Fe-oxidation rates (Fernandez-Rojo et al. 2018; Johnson et al. 2012). Optimal DO concentration varies depending on the identity of the FeOB. For example, the microaerophilic *Gallionella* thrive at lower oxygen conditions than other FeOB such as *Ferrovum* and *Leptospirillum* spp. (Hanert 2006; Johnson et al. 2012). Previous studies suggested that increasing oxygen concentrations may favor the development or activity of FeOB belonging to the *Ferrovum* genus (Fabisch et al. 2016; Fernandez-Rojo et al. 2018; Jwair et al. 2016). *Ferrovum* is often associated with the high Fe(II) concentration and high Fe oxidation rates, which explains its importance in AMD treatment (Chen et al. 2020; Johnson et al. 2014). The lower Fe(II) oxidation rate in period F and early period G had a negative impact on Fe precipitation, which decreased to less than 10%, but it did not significantly affect As removal, which remained similar ($\approx$ 70%) in period F (partial Fe(II) oxidation) and in period E (complete Fe(II) oxidation). This was attributed to the high As sorption and incorporation capacity of the Fe minerals that formed in the units; the sludge that formed under low DO supply in periods F and G exhibited an As/Fe molar ratio greater than 0.3. A high retention capacity was also observed in our previous field pilot that exhibited Fe oxidation yields below 20% (Fernandez-Rojo et al. 2019). This high As retention and As removal efficiency was probably promoted by the activity of As-oxidizing bacteria; it has been shown that some strains maintain the As oxidation activity at DO value around 1 mg/L (Gonzalez-Contreras et al. 2012; Hambsch et al. 1995).

Interruptions in operation affected Fe(II) oxidation efficiency in the early days after restart. This was indicative of a lag phase typical of biological processes and had been previously observed in biological Fe oxidation in batch and continuous flow experiments with AMD (Egal et al. 2009). Units shut down for several weeks converted the system into

a batch reactor. Under these conditions, when the substrate Fe(II) was no longer available, the Fe-oxidizing bacteria probably stopped growing and became dormant. During system restart, the bacteria need to recover their metabolism. Thus, shutoff periods had a negative effect for a short period of time (≤ 10 days) on pilot performance in terms of Fe(II) oxidation and subsequent As removal.

The flow rate increase from 15 to 30 L/h (HRT decrease from 18 to 9 h) between periods C and D decreased Fe(II) oxidation yield and Fe and As removal yields by ≈ 10%. This suggests that most of the reactions occurred within less than 9 h. Such relatively short hydraulic residence time fit with the ones reported in other studies for As-rich AMD treatment (Ahoranta et al. 2016). This suggests that the hydraulic residence time determined in the present study might be used to design a full-scale treatment.

Water temperature may affect the rate of biologically mediated reactions. Previous studies on bacterial strains oxidizing Fe or As isolated from polluted environments showed that their growth and oxidation activities were temperature dependent between 5 to 30 °C (Battaglia-Brunet et al. 2002; Dopson et al. 2006; Ito et al. 2012; Kim et al. 2008). Tardy et al. (2018) reported that water temperature greater than 20 °C stimulate As oxidation mediated by autochthonous bacterial communities in the Carnoulès AMD water. In our experiments, water temperature ranged from 5 to 27 °C; however, the variation did not correlate directly with Fe or As removal yields. More data would be required to confirm a possible temperature dependency for biological As and Fe oxidation in the systems.

Sludge Composition and Control of Outlet Water Physico-chemistry

Jarosite, gypsum and quartz were identified by XRD in the sludge under routine operation (periods A–E). Quartz originated from the waste pile (Fernandez-Rojo et al. 2019). The presence of jarosite at pH ≤ 2.8–3.0 is in agreement with the stability domain of this mineral (Bigham et al., 1996; Sánchez-España et al., 2011). Jarosite has been described as an As scavenger under acidic and sulfate-rich conditions (Asta et al. 2009; Johnston et al. 2012; Kendall et al. 2013). This retention is associated with an initial co-precipitation of As(V) with Fe(III), which is often completed by the replacement of the sulfate groups of jarosite with the As(V) present in solution (Shi et al. 2021). However, jarosite is often considered to have formed by recrystallization of schwertmannite (Asta et al. 2010a, b). Wang et al. (2006) reported the transformation of schwertmannite to jarosite with aging. Burton et al. (2021) recently found that increasing levels of As(V) incorporation within schwertmannite enhanced also the transformation of schwertmannite to jarosite. In our previous studies, the formation of As-poor jarosite from the Carnoulès AMD occurred after a first precipitation step of tooeleite ($Fe_6(AsO_3)_4SO_4(OH)_4{\cdot}4H_2O$) or As(III)-schwertmannite (Duquesne et al. 2003). Tooeleite was not evidenced in the present study, probably due to the rapid Fe(II) oxidation and subsequent achievement of lower As(III)/Fe(III) molar ratios in the solid. The reported As/Fe ≤ 0.5 ratio in the sludge of the present field pilot test did not fit the stoichiometric formula of tooeleite (As/Fe = 0.67).

In general, the sorption capacity reported for jarosite is considerably less than that reported for schwertmannite or amorphous phases. Asta et al. (2009) reported that at initial As concentration of 100 mg/L in water, As(V) sorption capacity of synthetic jarosite of 21 mg/g at pH 1.5–2.5. Ahoranta et al. (2016) estimated that the highest As(III) and As(V) sorption capacities of biogenic jarosite at pH 3.0 were 1.24 and 2.07 mg/g, respectively. For comparison, the sorption capacity of schwertmannite at pH 3 has been estimated at 0.31–0.33 mol As(V)/mol Fe, corresponding to more than 200 mg As(V)/g (Burton et al. 2009; Carlson et al. 2002). In the present study, the As content in the sludge ranged between 39 and 91 mg/g, corresponding to As/Fe molar ratio of 0.3 ± 0.08 (Table 1), which implies the contribution of an amorphous phase for As retention.

The calculated SI indicated that As(V) solubility in most of the outlet water samples was likely to be controlled by amorphous scorodite or AFA (Table 4). This confirms the findings of Langmuir et al. (2006), who highlighted the role of AFA in the control of As mobility in mine tailings. Occurrence of this phase is also a common observation under microbially-active AMD conditions (Fernandez-Rojo et al. 2018; Maillot et al. 2013). Therefore, amorphous schwertmannite and amorphous ferric arsenate were probably the dominant phases responsible for As removal in our field units. The As removal performance was probably limited by the solubility of amorphous ferric arsenate at pH 2.8 ± 0.3. Slightly positive SI values and occurrence of As(V) colloids suggest that kinetics play a role in the precipitation of the Fe/As phases.

Conclusions and Perspectives

During more than a year of functioning, we obtained nearly complete Fe(II) oxidation and up to 80% As removal during all seasons in the two treatment units (PS and WP supports), despite variations in the Carnoulès AMD hydrochemistry. The rates of biological Fe oxidation were similar to laboratory rates and to those reported for AMD streams worldwide. The As removal yields were greater and more stable than in our previous field pilot and similar to the laboratory bioreactor. The WP bacterial support provided shorter delay before performance recovery. The sludge composition was stable throughout time and similar in the PS and WP systems. The

predominance of arsenate phases is a positive outcome in the perspective of long term storage. Hence, the robustness of the treatment regarding seasonal variations of AMD physical-chemistry, environmental and operational conditions suggests great potential for further scale-up and extrapolation of the treatment to other AMD with similar properties.

Further work will focus on additional treatments (sulfate reducing bioreactor, limestone channel) to improve the quality of the treated mine water. Research is in progress to characterize the bacterial diversity in the units, particularly the genetic potential for As oxidation, which is a key process for As immobilization.

Supplementary Information The online version contains supplementary material available at https://doi.org/10.1007/s10230-022-00885-4.

Acknowledgements The authors acknowledge the financial support of (ADEME) [APR-GESIPOL-2017-COMPAs], the Occitanie region, and BRGM for co-funding of the PhD grant of Camila Diaz-Vanegas, and OSU-OREME for co-funding of the long-term monitoring of Carnoulès AMD physico-chemistry. Thanks to Adam Djibrine and Amandine Malcles for their work during experimental monitoring. Thanks to Jérémy Engevin for bringing his expertise on the design and installation of the devices and to Rémi Freydier, Léa Causse, and Sophie Delpoux for their help in analytical work on the AETE-ISO platform, OSU OREME, Université de Montpellier. The authors would like to thank the editors for their contribution to improve the quality of the manuscript.

References

Ahoranta SH, Kokko ME, Papirio S, Özkaya B, Puhakka J (2016) Arsenic removal from acidic solutions with biogenic ferric precipitates. J Hazard Mater 306:124–132. https://doi.org/10.1016/j.jhazmat.2015.12.012

Asta MP, Cama J, Martínez M, Giménez J (2009) Arsenic removal by goethite and jarosite in acidic conditions and its environmental implications. J Hazard Mater 171:965–972. https://doi.org/10.1016/j.jhazmat.2009.06.097

Asta MP, Ayora C, Acero P, Cama J (2010a) Field rates for natural attenuation of arsenic in Tinto Santa Rosa acid mine drainage (SW Spain). J Hazard Mater 177:1102–1111. https://doi.org/10.1016/j.jhazmat.2010.01.034

Asta MP, Ayora C, Román-Ross G, Cama J, Acero GA, Charnock J, Bardelli F (2010b) Natural attenuation of arsenic in the Tinto Santa Rosa acid stream (Iberian Pyritic Belt, SW Spain): the role of iron precipitates. Chem Geol 271:1–12. https://doi.org/10.1016/j.chemgeo.2009.12.005

Battaglia-Brunet F, Dictor M-C, Garrido F, Crouzet C, Morin D, Dakeyser K, Clarens M, Baranger P (2002) An arsenic(III)-oxidizing bacterial population: selection, characterization, and performance in reactors. J Appl Microbiol 93:656–667. https://doi.org/10.1046/j.1365-2672.2002.01726.x

Bigham J, Schwertmann U, Traina J, Winland R, Wolf M (1996) Schwertmannite and the chemical modeling of iron in acid sulfate waters. Geochim Cosmochim Acta 60:2111–2121

Blanc P, Lassin A, Piantone P, Azaroual M, Jacquemet N, Fabbri A, Gaucher E (2012) Thermoddem: a geochemical database focused on low temperature water/rock interactions and waste materials. Appl Geochem 27:2107–2116. https://doi.org/10.1016/j.apgeochem.2012.06.002

Bruneel O, Personné JC, Casiot C, Leblanc M, Elbaz-Poulichet F, Mahler B, Le Flèche A, Grimont P (2003) Mediation of arsenic oxidation by *Thiomonas* sp. in acid-mine drainage (Carnoulès, France). J Appl Microbiol 95:492–499. https://doi.org/10.1046/j.1365-2672.2003.02004

Burton ED, Bush RT, Johnston S, Watling K, Hocking R, Sullivan L, Parker G (2009) Sorption of arsenic(V) and arsenic(III) to schwertmannite. Environ Sci Technol 43:9202–9207. https://doi.org/10.1021/es902461x

Burton ED, Karimian N, Johnston S, Schoepfer V, Choppala G, Lamb D (2021) Arsenic-imposed effects on schwertmannite and jarosite formation in acid mine drainage and coupled impacts on arsenic mobility. ACS Earth Sp Chem 5:1418–1435. https://doi.org/10.1021/acsearthspacechem.1c00047

Carlson L, Bigham JM, Schwertmann U, Kyek A, Wagner F (2002) Scavenging of As from acid mine drainage by schwertmannite and ferrihydrite: a comparison with synthetic analogues. Environ Sci Technol 36:1712–1719. https://doi.org/10.1021/es010271

Casiot C, Leblanc M, Bruneel O, Personné J, Koffi K, Elbaz-Poulichet F (2003) Geochemical processes controlling the formation of As-rich waters within a tailings impoundment (Carnoulès, France). Aquat Geochem 9:273–290. https://doi.org/10.1023/B:AQUA.0000028985.07557.39

Chen CJ, Jiang WT (2012) Influence of waterfall aeration and seasonal temperature variation on the iron and arsenic attenuation rates in an acid mine drainage system. Appl Geochem 27:1966–1978. https://doi.org/10.1016/j.apgeochem.2012.06.003

Chen H, Xiao T, Ning Z, Li Q, Xiao E, LiuY XQ, Lan X, Ma L, Lu F (2020) In-situ remediation of acid mine drainage from abandoned coal mine by filed pilot-scale passive treatment system: performance and response of microbial communities to low pH and elevated Fe. Bioresour Technol 317:123985. https://doi.org/10.1016/j.biortech.2020.123985

Dopson M, Halinen A-K, Rahunen N, Ozkaya B, Sahinkaya E, Kaksonen A, Lindstrom B, Puhakka J (2006) Mineral and iron xidation at low temperatures by pure and mixed cultures of acidophilic microorganisms. Biotechnol Bioeng 97:1205–1215. https://doi.org/10.1002/bit.21312

Duquesne K, Lebrun S, Casiot C, Bruneel O, Leblanc M, Morin G, Bonnefoy V (2003) Immobilization of Arsenite and Ferric Iron by 69:6165–6173. https://doi.org/10.1128/AEM.69.10.6165

Egal M, Casiot C, Morin G, Parmentier M, Bruneel O, Lebrun S, Elbaz-Poulichet F (2009) Kinetic control on the formation of tooeleite, schwertmannite and jarosite by *Acidithiobacillus ferrooxidans* strains in an As(III)-rich acid mine water. Chem Geol 265:432–441. https://doi.org/10.1016/j.chemgeo.2009.05.008

Egal M, Casiot C, Morin G, Elbaz-Poulichet F, Cordier M, Bruneel O (2010) An updated insight into the natural attenuation of As concentrations in Reigous Creek (southern France). Appl Geochem 25:1949–1957. https://doi.org/10.1016/j.apgeochem.2010.10.012

Elbaz-Poulichet F, Bruneel O, Casiot C (2006) The Carnoules mine. Generation of As-rich acid mine drainage, natural attenuation processes and solutions for passive in-situ remediation. Difpolmine (Diffuse Pollut From Min Act) Montpellier, France. hal-00184269

Fabisch M, Freyer G, Johnson C, Büchel G, Akob D, Neu T, Küsel K (2016) Dominance of "*Gallionella capsiferriformans*" and heavy metal association with *Gallionella*-like stalks in metal-rich pH 6 mine water discharge. Geobiology 14:68–90. https://doi.org/10.1111/gbi.12162

Fernandez-Rojo L, Héry M, Le Pape P, Braungardt C, Desoeuvre TE, Tardy V, Resongles E, Laroche DS, Joulian C, Battaglia-Brunet F, Boisson J, Graphin G, Morin G, Casiot C (2017) Biological attenuation of arsenic and iron in a continuous flow bioreactor

treating acid mine drainage (AMD). Water Res 123:594–606. https://doi.org/10.1016/j.watres.2017.06.059

Fernandez-Rojo L, Casiot C, Tardy V, Laroche E, Le Pape P, Morin G, Joulian B-B, Braungardt C, Desoeuvre A, Delpoux S, Boisson J, Héry M (2018) Hydraulic retention time affects bacterial community structure in an As-rich acid mine drainage (AMD) biotreatment process. Appl Microbiol Biotechnol 102:9803–9813. https://doi.org/10.1007/s00253-018-9290-0

Fernandez-Rojo L, Casiot C, Laroche E, Tardy V, Bruneel O, Delpoux S, Desoeuvre A, Grapin G, Savignac J, Boisson J, Morin G, Battaglia-Brunet F, Joulian C, Héry M (2019) A field-pilot for passive bioremediation of As-rich acid mine drainage. J Environ Manage 232:910–918. https://doi.org/10.1016/j.jenvman.2018.11.116

Garcia-Rios M, De Windt L, Luquot L, Casiot C (2021) Modeling of microbial kinetics and mass transfer in bioreactors simulating the natural attenuation of arsenic and iron in acid mine drainage. J Hazard Mater 405:124133. https://doi.org/10.1016/j.jhazmat.2020.124133

Gonzalez-Contreras P, Weijma J, Buisman C (2012) Bioscorodite crystallization in an airlift reactor for arsenic removal. Cryst Growth Des 12:2699–2706. https://doi.org/10.1021/cg300319s

Habe H, Sato Y, Aoyagi T, Inaba T, Hori T, Hamai T, Hayashi K, Kobayashi M, Sakata T, Sato N (2020) Design, application, and microbiome of sulfate-reducing bioreactors for treatment of mining-influenced water. Appl Microbiol Biotechnol 104:6893–6903. https://doi.org/10.1007/s00253-020-10737-2

Hambsch B, Raue B, Brauch H (1995) Determination of arsenic(III) for the investigation of the microbial oxidation of arsenic(III) to arsenic(V). Acta Hydrochim Hydrobiol 4:166–172. https://doi.org/10.1002/aheh.19950230404

Hanert HH (2006) The *Genus Gallionella*. In: Dworkin M, Falkow S, Rosenberg E, Schleifer K, Stackerbrandt E (eds) The prokaryotes: volume 7: proteobacteria: delta, epsilon subclass. Springer, New York, pp 990–995

Igarashi T, Herrera P, Uchiyama H, Miyamae H, Iyatomi N, Barltazar HK (2020) The two-step neutralization ferrite-formation process for sustainable acid mine drainage treatment: removal of copper, zinc and arsenic, and the influence of coexisting ions on ferritization. Sci Total Environ 715:136877. https://doi.org/10.1016/j.scitotenv.2020.136877

Ito A, Miura J, Ishikawa N, Umita T (2012) Biological oxidation of arsenite in synthetic groundwater using immobilised bacteria. Water Res 46:4825–4831. https://doi.org/10.1016/j.watres.2012.06.013

Johnson DB, Kanao T, Hedrich S (2012) Redox transformations of iron at extremely low pH: Fundamental and applied aspects. Front Microbiol 3:1–13. https://doi.org/10.3389/fmicb.2012.00096

Johnson DB, Hallberg KB, Hedrich S (2014) Uncovering a microbial enigma: isolation and characterization of the streamer-generating, iron-oxidizing, acidophilic bacterium "Ferrovum myxofaciens." Appl Environ Microbiol 80:672–680. https://doi.org/10.1128/AEM.03230-13

Johnston SG, Burton ED, Keene A, Planer-Friedrich B, Voegelin A, Blackford M, Lumpkin G (2012) Arsenic mobilization and iron transformations during sulfidization of As(V)-bearing jarosite. Chem Geol 334:9–24. https://doi.org/10.1016/j.chemgeo.2012.09.045

Jwair RJ, Tischler JS, Janneck E, Schlömann M (2016) Acid mine water treatment using novel acidophilic iron-oxidizing bacteria of the genus "Ferrovum": effect of oxygen and carbon dioxide on survival. In: Drebenstedt C, Paul M (eds.), Proc, IMWA 2016, pp 1060–1063. www.imwa.info/docs/imwa_2016/IMWA2016_Jwair_85.pdf

Kendall MR, Madden AS, Elwood Madden ME, Hu Q (2013) Effects of arsenic incorporation on jarosite dissolution rates and reaction products. Geochim Cosmochim Acta 112:192–207. https://doi.org/10.1016/j.gca.2013.02.019

Kim DJ, Pradhan D, Park KH, Ahn J, Lee S (2008) Effect of pH and temperature on iron oxidation by mesophilic mixed iron oxidizing microflora. Mater Trans 49:2389–2393. https://doi.org/10.2320/matertrans.MER2008051

Langmuir D, Mahoney J, Rowson J (2006) Solubility products of amorphous ferric arsenate and crystalline scorodite ($FeAsO_4{\cdot}2H_2O$) and their application to arsenic behavior in buried mine tailings. Geochim Cosmochim Acta 70:2942–2956. https://doi.org/10.1016/j.gca.2006.03.006

Laroche E, Casiot C, Fernandez-Rojo L, Desoeuvre A, Tardy V, Bruneel O, Battaglia-Brunet F, Joulian C, Héry M (2018) Dynamics of bacterial communities mediating the treatment of an As-rich acid mine drainage in a field pilot. Front Microbiol 9:3169. https://doi.org/10.3389/fmicb.2018.03169

Larson L, Sa J, Kaley B, Sheng Y, Bibby K, Burgos W (2014) Thermodynamic controls on the kinetics of microbial low-pH Fe(II) oxidation. Sci Technol 48:9246–9254. https://doi.org/10.1021/es501322d

Leblanc M, Casiot C, Elbaz-Poulichet F, Personnè C (2002) Arsenic removal by oxidizing bacteria in a heavily arsenic-contaminated acid mine drainage system (Carnoulès, France). Geol Soc Spec Publ 198:267–274. https://doi.org/10.1144/GSL.SP.2002.198.01.17

Maillot F, Morin G, Juillot F, Bruneel O, Casiot C, Ona-Nguema G, Wang Y, Lebrun S, Aubry E, Vlaic G, Brown J (2013) Structure and reactivity of As (III)- and As(V)-rich schwertmannites and amorphous ferric arsenate sulfate from the Carnoulès acid mine drainage, France: comparison with biotic and abiotic model compounds and implications for As remediation. Geochim Cosmochim Acta 104:310–329. https://doi.org/10.1016/j.gca.2012.11.016

Majzlan J, Lalinská B, Chovan M, Jurkovicˇ L, Milovská S, Göttlicher J (2007) The formation, structure, and ageing of As-rich hydrous ferric oxide at the abandoned Sb deposit Pezinok (Slovakia). Geochim Cosmochim Acta 71:4206–4220. https://doi.org/10.1016/j.gca.2007.06.053

Majzlan J, Dachs E, Benisek A, Koch C, Bolanz R, Göttlicher J, Steininger R (2016) Thermodynamic properties of tooeleite, $Fe_6^{3+}(As_3{+}O_3)4(SO_4)(OH)_4{\cdot}4H_2O$. Chem Erde 76:419–428. https://doi.org/10.1016/j.chemer.2016.05.001

Mondal P, Majumder C, Mohanty B (2006) Laboratory based approaches for arsenic remediation from contaminated water: recent developments. J Hazard Mater 137:464–479. https://doi.org/10.1016/j.jhazmat.2006.02.023

Morin G, Juillot F, Casiot C, Bruneel O, Personné J, Elbaz-Poulichet F, Leblanc M, Ildefonse P, Calas G (2003) Bacterial formation of tooeleite and mixed arsenic(iii) or arsenic(v)—iron(III) gels in the Carnoulès acid mine drainage, France. A XANES, XRD, and SEM study. Environ Sci Technol 37:1705–1712. https://doi.org/10.1021/es025688p

Neculita C, Zagury G, Bruno B (2007) Passive treatment of acid mine drainage in bioreactors using sulfate-reducing bacteria: critical review and research needs. J Environ Qual 31:1–16. https://doi.org/10.2134/jcq200

Nordstrom DK, Alpers CN (1999) Goechemistry of acid mine waters. In: Plumlee G, Logsdon M (eds) Reviews in economic geology, volume 6A: the environmental geochemistry of mineral deposits, part A: processes, techniques, and health issues. Society of Economic Geologists, New York, pp 133–156

Paikaray S (2015) Arsenic geochemistry of acid mine drainage. Mine Water Environ 34:181–196. https://doi.org/10.1007/s10230-014-0286-4

Pesic B, Oliver D (1989) An electrochemical method of measuring the oxidation rate of ferrous to ferric iron with oxygen in the presence

of *Thiobacillus ferrooxidans*. Biotech BioEng 33(4):428–439. https://doi.org/10.1002/bit.260330408

Resongles E, Le Pape P, Fernandez-Rojo L, Morin DS, Brest J, Guo S, Casiot C (2016) Routine determination of inorganic arsenic speciation in precipitates from acid mine drainage using orthophosphoric acid extraction followed by HPLC-ICP-MS. Anal Methods 8:7420–7426. https://doi.org/10.1039/c6ay02084d

Ribeiro A, Simões De Carvalho P, Horta M, da Silva C, Tavares dos Santos A, Cuhna P, Costa M (2016) Spatial variability of soils and stream sediments and the remediation effects in a Portuguese uranium mine area. Chem Erde 76:501–518. https://doi.org/10.1016/j.chemer.2016.08.003

Rötting T, Caraballo M, Serrano J, Ayora C, Carrera J (2008a) Field application of calcite dispersed alkaline substrate (calcite-DAS) for passive treatment of acid mine drainage with high Al and metal concentrations. Appl Geochem 23:1660–1674. https://doi.org/10.1016/j.apgeochem.2008.02.023

Rötting T, Thomas R, Ayora C, Carrera J (2008b) Passive treatment of acid mine drainage with high metal concentrations using dispersed alkaline substrate. J Environ Qual 37:1741–1751. https://doi.org/10.2134/jeq2007.0517

Sánchez-España J, Yusta I, Diez-Ercilla M (2011) Schwertmannite and hydrobasaluminite: a re-evaluation of their solubility and control on the iron and aluminium concentration in acidic pit lakes. Appl Geochem 26:1752–1774. https://doi.org/10.1016/j.apgeochem.2011.06.020

Sato Y, Hamai T, Hori T, Habe H, Kobayashi M, Sakata T (2018) Year-round performance of a passive sulfate-reducing bioreactor that uses rice bran as an organic carbon source to treat acid mine drainage. Mine Water Environ 37:586–594. https://doi.org/10.1007/s10230-017-0489-6

Sheng Y, Kaley B, Bibby K, Grettenberger C, Macalady J, Wang G, Burgos W (2017) Bioreactors for low-pH iron(II) oxidation remove considerable amounts of total iron. RSC Adv 7:35962–35972. https://doi.org/10.1039/c7ra03717a

Shi M, Min X, Ke Y, Lin Z, Yang Z, Wang S, Peng N, Yan X, Luo S, Wu J, Wei Y (2021) Recent progress in understanding the mechanism of heavy metals retention by iron (oxyhydr)oxides. Sci Total Environ 752:141930. https://doi.org/10.1016/j.scitotenv.2020.141930

Tardy V, Casiot C, Fernandez-Rojo L, Resongles E, Desoeuvre A, Joulian C, Battaglia-Brunet F, Héry M (2018) Temperature and nutrients as drivers of microbially mediated arsenic oxidation and removal from acid mine drainage. Appl Microbiol Biotechnol 102:2413–2424. https://doi.org/10.1007/s00253-017-8716-4

Tsai SL, Singh S, Chen W (2009) Arsenic metabolism by microbes in nature and the impact on arsenic remediation. Curr Opin Biotechnol 20:659–667. https://doi.org/10.1016/j.copbio.2009.09.013

van der Lee J, De Windt L, Lagneau V, Goblet P (2003) Module-oriented modeling of reactive transport with HYTEC. Comput Geosci 29:265–275. https://doi.org/10.1016/S0098-3004(03)00004-9

Wang H, Zeng Y, Guo C, Bao Y, Lu G, Reinfelder J, Dang Z (2018) Bacterial, archaeal, and fungal community responses to acid mine drainage-laden pollution in a rice paddy soil ecosystem. Sci Total Environ 616–617:107–116. https://doi.org/10.1016/j.scitotenv.2017.10.224

Whitehead PG, Hall G, Neal C, Prior H (2005) Chemical behaviour of the Wheal Jane bioremediation system. Sci Total Environ 338:41–51. https://doi.org/10.1016/j.scitotenv.2004.09.004